JOURNAL OF GUIDANCE, CONTROL, AND DYNAMICS
Vol. 30, No. 5, September–October 2007

Predictive Guidance for Pursuit–Evasion Engagements Involving Multiple Decoys

D. Dionne*
Lockheed Martin Canada, Montreal, Quebec H4P 1K6, Canada
H. Michalska†
McGill University, Montreal, Quebec H3A 2A7, Canada
and
C. A. Rabbath‡
Defence Research and Development Canada—Valcartier, Val-Belair, Quebec G3J 1X5, Canada

DOI: 10.2514/1.25481

A guidance law is developed for situations in which the pursuer's command is 1) conditioned on a multimodal probability density function of the target state, and 2) constrained by a bounded control effort. The novel law adopts a predictive control approach with two horizons: a fixed cost horizon, and a receding control horizon. The law performs a first optimization over the fixed cost horizon to deliver a novel control constraint. This control constraint is then employed in a new open-loop optimization procedure to deliver a piecewise-constant open-loop controller that is optimal over the receding control horizon. When the density function is unimodal, the novel law is proven to be equivalent to other approaches in feedback with the average of the density function (i.e., the minimum mean square error estimate, as suggested by the certainty equivalence principle), or the maximizer of the density function (i.e., the maximum a posteriori probability estimate). In an example engagement scenario with decoys, the novel law demonstrates a higher probability of interception than comparable laws in feedback with the minimum mean square error or maximum a posteriori probability estimates.

I. Introduction

THE problem of intercepting a moving target has been studied extensively; see the reviews in [1,2]. These studies demonstrated that the interception of a target was feasible in several cases involving partial information on the target state, uncertainties in the dynamics, and limited maneuverability of the interceptor and target [1]. Similarly, it was shown that an effective mean of evasion for the target is to generate a sudden shift in its apparent position; see Chapter 20 in [2]. Such a shift in the apparent position can be generated by the deployment of a decoy having a signature similar to that of the target [3]. The apparent sudden shift occurs at the instant when the pursuer discriminates between the decoy and the target. Passive homing, which depends only on the target as a source of tracking energy, is particularly susceptible to such decoy countermeasures as seen in Chapter 15 of [4].

The interception problem was also studied for cases when the available information on the target takes the form of a non-Gaussian probability density function (PDF) [5–9]. The resulting controllers did not assume validity of the separation and certainty equivalence principles; that is, the controllers were a function of the whole PDF (rather than the average value of the PDF). Such controllers are known to be optimal for a broad class of systems [10]. In [5,6], a non-Gaussian PDF was first calculated using a multiple model state estimator. Best and Norton [5] then developed a predictive control formulation without hard constraints on the control effort, while hard constraints were assumed in [6]. In [7,8], the non-Gaussian PDF was first calculated using a particle filter, a game formulation of the control problem was adopted, and a controller respecting the hard constraint on the control effort was obtained by application of a simulation technique similar to particle filtering. In [9], a multimodal PDF is generated by the presence of a decoy, and preliminary results of a new predictive guidance law for this situation are presented.

This paper presents a novel predictive guidance law that extends [6,9] by the introduction of a new piecewise-constant optimal control command, a new bound on the temporal evolution of the PDF, and a new technique to ensure uniqueness of the solution. This paper also extends previous simulation results by the study of engagement scenarios involving multiple decoys, and by the comparison of the results with those from both receding and nonreceding guidance laws. The objective of the novel guidance law is the maximization of the probability that the target's position lies within the reachable set of the interceptor. In the presence of undiscriminated decoys (that generates a multimodal PDF of the target's position), this guidance objective has the consequence of maintaining the undiscriminated target and decoys in the reachable set of the interceptor for as long as possible. The benefits of such behavior are that 1) the need for discrimination is delayed while both target and decoys are in the interceptor's reachable set, hence relaxing the constraints on the discriminator, 2) increased information can be gathered before discrimination, and 3) the probability of a successful interception can be improved. In simulated engagements, the homing performance of the novel guidance law is compared to that of laws in which the interceptor is steered toward 1) the minimum mean square error (MMSE) estimate of the target position (which can be located between the modes, i.e., a point of low probability of target presence), and 2) the maximum a posteriori probability (MAP) estimate of the target position.

II. Problem Statement

Consider a planar interception problem involving an interceptor and a target. The target launches decoys at unknown time instants. To the interceptor, these decoys appear as apparent targets. The

Received 28 May 2006; revision received 1 April 2007; accepted for publication 10 April 2007.

*Ph.D. Engineer, Research and Development Department.
†Associate Professor, Electrical Engineering Department.
‡Defence Scientist, DRDC, 2459 Pie-XI Blvd. North; also at Mechanical Engineering Department, McGill University, Montreal, Quebec H3A 2A7, Canada. Professional Member AIAA.

interceptor has to discriminate between the decoys and the target because it is assumed that the interceptor can intercept only one of the apparent targets.

Let S be a set of N decoys deployed during the engagement, $S = \{1, \ldots, N\}$, where the value of N is unknown to the interceptor. The decoy $i \in S$ is deployed at instant t^i_{start} and is discriminated at instant t^i_{end}. A simplified planar representation of this scenario is given by

$$\dot{x}_I(t) = A_I(t)x_I(t) + B_I(t)u(t) \tag{1a}$$

$$\dot{x}_T(t) = g(x_T, a, t, w) \tag{1b}$$

$$\dot{x}^i_S(t) = d\left(x^i_S, t, v^i, t^i_{\text{start}}, t^i_{\text{end}}\right), \qquad i \in S \tag{1c}$$

$$y(t_k) = h\left(x_T, x^1_S, \ldots, x^N_S, t_k, \eta\right), \qquad t_k \triangleq k\Delta, k = 0, 1, \ldots \tag{1d}$$

where $x_I(t) \in \mathbb{R}^p$, $x_T(t) \in \mathbb{R}^e$, and $x^i_S(t) \in \mathbb{R}^d$ are the state of the interceptor, of the target, and of the decoy $i \in S$, respectively; $u(t) \in \mathbb{R}^1$ and $a(t) \in \mathbb{R}^1$ are the interceptor and target control commands; and $y(t_k) \in \mathbb{R}^y$ is a discrete measurement (sampling period Δ) on the state of the target and of the decoys. Without loss of generality, the engagement is assumed to start at $t = 0$. The functions A_I and B_I are assumed continuous, and the functions g, d, and h are assumed to satisfy sufficient observability conditions to allow for the reconstruction (in the form of a PDF) of the target's and the decoy's states from the measurements. The uncertain dynamics of the target and decoys are represented by the independent process noises w and v^i, $i \in S$, while the uncertainty on the measurement is represented by the noise η. These noises are assumed to have a known distribution given by $w \sim p(w)$, $v^i \sim p(v^i)$, and $\eta \sim p(\eta)$. The control signals u and a are assumed bounded by $u^{\max}$ and $a^{\max}$, respectively,

$$|u(\tau)| \le u^{\max}, \qquad |a(\tau)| \le a^{\max}, \qquad \tau \ge 0 \tag{2}$$

Let $z_I \in \mathbb{R}^1$ and $z_T \in \mathbb{R}^1$ be the lateral position (in the inertial frame of the interceptor, orthogonal to the initial line of sight) of the interceptor and target at the intercept time t_f.

$$z_I \triangleq D_I x_I(t_f), \qquad D_I \triangleq [1\ 0\ \cdots\ 0] \in \mathbb{R}^p \tag{3a}$$

$$z_T \triangleq D_T x_T(t_f), \qquad D_T \triangleq [1\ 0\ \cdots\ 0] \in \mathbb{R}^e \tag{3b}$$

The value of t_f is assumed known. The guidance objective is to steer the interceptor to achieve $z_I = z_T$. The variable z_I is deterministic (it results from the interceptor's strategy u), while z_T is a random variable (due to the uncertain target position).

III. Guidance Approach

A predictive guidance approach is adopted that steers the interceptor toward the predicted position of the target at the intercept time. This approach involves reconstructing the target's state from the measurements and predicting its lateral position at the intercept time. Without engaging in data association, filtering, and prediction issues, the end result of the reconstruction is an estimation of z_T in the form of a PDF denoted $p(z_T \mid \mathcal{Y}^k)$, where $\mathcal{Y}^k$ is the σ algebra generated by the measurements $\mathcal{Y}^k \triangleq \sigma\{y(t_s)\colon 0 < s \le k\}$. This PDF is recalculated at each instant t_k when new measurements arrive. The presence of a decoy is relevant to the control problem only at times when it affects the density $p(z_T \mid \mathcal{Y}^k)$.

The proposed control approach is illustrated in Fig. 1 and is formulated to maximize the probability of the target remaining reachable despite the interceptor having a bounded control effort, and despite that the density $p(z_T \mid \mathcal{Y}^k)$ 1) evolves in time with the arrival of new measurements, 2) may be multimodal, and 3) may abruptly change (because a decoy gets discriminated). This control approach involves a sequence of two optimization problems to be solved at any instant t_k. A first optimization problem is solved over the fixed cost horizon t_f to deliver an optimal receding control constraint. Then a second optimization problem is solved over the receding time interval $[t_k, t_{k+1}]$ to deliver an open-loop control command satisfying the receding control constraint. The receding control constraint is an estimate calculated from $p(z_T \mid \mathcal{Y}^k)$ and is new in that it explicitly accounts for the limited control effort of the interceptor while optimizing the probability of the target remaining reachable as seen in Sec. III.A. The open-loop control command is calculated by the introduction of a novel optimization technique in $\mathcal{L}^2[t_k, t_{k+1}]$ that delivers an optimal piecewise-constant open-loop control command over the receding horizon as seen in Sec. III.B.

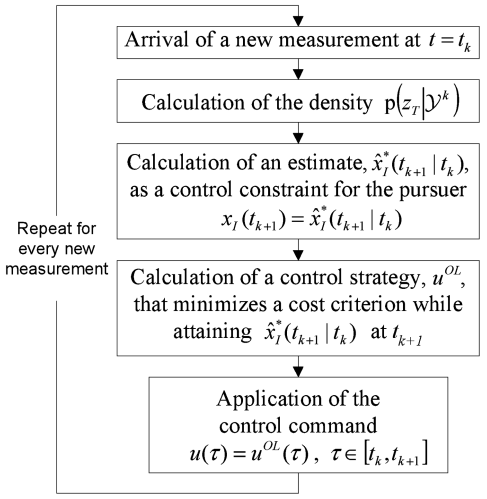

Fig. 1 Flow diagram of the proposed predictive guidance law. The estimate $x^*_I(t_{k+1} \mid t_k)$ is the maximizer of Eq. (9) in Sec. III.A, and the open-loop control command u^{OL} is given in Sec. III.B.

A. Calculation of the Receding Control Constraint

The receding control constraint is a state to be reached by the interceptor at the end of the receding control horizon. The constraint is selected to account for 1) the bounded control effort of the interceptor, and 2) a bound $\gamma(t_k)$ about the future temporal evolution of the density $p(z_T \mid \mathcal{Y}^k)$. Whenever possible, the receding control constraint is selected to maximize the probability of the target remaining in the reachable set of the interceptor.

The bound γ is first characterized. Next, sets are defined, followed by the statement of the optimization problem. Finally, the uniqueness of the optimal solution is addressed.

1. *Bound About the Temporal Evolution of the Density*

The bound about the future temporal evolution of the PDF is defined by comparison of two densities: the (known) current PDF $p(z_T \mid \mathcal{Y}^k)$ and a (unknown) PDF $p(z_T \mid \mathcal{Y}^f)$ conditioned on all the past and future measurements. Let these densities be described by M modes (each mode is understood as a peak in the PDF),[§] and let c_i be the maximum of mode $i \in \{1, \ldots, M\}$. Then, an upper bound on the temporal evolution of the density from instants t_k to t_f is given by the maximum displacement of the peaks, that is,

$$\gamma(t_k) > \max_{i \in \{1, \ldots, M\}} |c_i(z_T \mid \mathcal{Y}^f) - c_i(z_T \mid \mathcal{Y}^k)| \tag{4}$$

It is assumed that the bound $\gamma(t_k)$ is known.[¶]

2. *Definition of Useful Sets*

Let us define $\Re(t_{k+1}, x_I(t_k))$ as the set of states reachable by the interceptor at the next time instant t_{k+1} given that the state at time instant t_k is $x_I(t_k)$. The set $\Re(t_{k+1}, x_I(t_k))$ satisfies the bound on the

[§]The M Gaussian densities of a multiple model estimator generates such a multimodal PDF.

[¶]The actual determination of $\gamma(t_k)$ is heuristic; an example is provided in Sec. V.

control effort of the interceptor and any of the admissible points $x_I(t_{k+1} \mid t_k) \in \Re(t_{k+1}, x_I(t_k))$ is an admissible receding control constraint.

Let $\beta(t_f, x_I(t_{k+1} \mid t_k))$ be the set of positions reachable by the interceptor at time instant t_f given that the state was $x_I(t_{k+1} \mid t_k)$ at time instant t_{k+1}, that is,

$$\beta(t_f, x_I(t_{k+1} \mid t_k)) \triangleq D_I \Re(t_f, x_I(t_{k+1} \mid t_k)) = [z^c - r, z^c + r] \quad (5)$$

Each β set is in the form of an interval with a center point z^c and with a measure $2r$.

Let $\bar{\beta}$ be a subinterval of a β set and let it be given by

$$\bar{\beta}(t_f, x_I(t_{k+1}|t_k)) \triangleq [z^c - \bar{r}, z^c + \bar{r}], \quad \text{if } \bar{r} > 0 \quad (6)$$

with $\bar{r}(t_k) \triangleq r(t_k) - \gamma(t_k)$, and where z^c and r are calculated in Eq. (5). The reduced measure $\bar{r}$ accounts for future, bounded, temporal variations in the density $p(z_T \mid \mathcal{Y}^k)$.

3. Optimization Problem

The receding control constraint is

$$x_I(t_{k+1}) = \hat{x}_I^\star(t_{k+1} \mid t_k) \quad (7)$$

where $\hat{x}_I^\star$ is a state to be reached at the end of the receding control horizon. The optimization problem is about finding a feasible $\hat{x}_I^\star(t_{k+1} \mid t_k)$ that is optimal at the cost horizon t_f

$$\hat{x}_I^\star(t_{k+1} \mid t_k) = \arg \max_{x_I(t_{k+1}|t_k) \in \Re} U(x_I(t_{k+1} \mid t_k)) \quad (8)$$

where $\Re$ is the set of reachable states, and $U \in \mathbb{R}^1$ is the utility at the cost horizon t_f

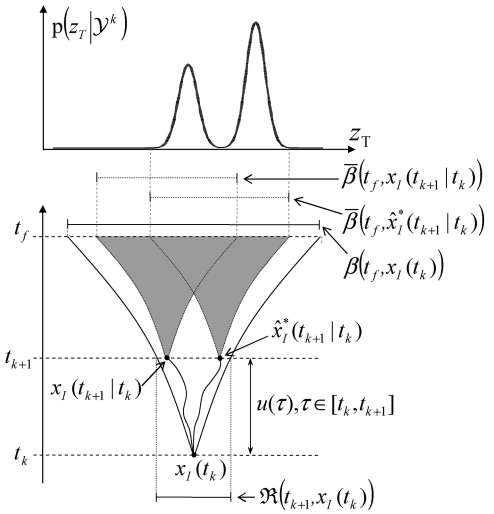

Fig. 2 Optimization problem and evolution of the reachable sets under the action of the control $u(\tau)$, $\tau \in [t_k, t_{k+1}]$. The upper panel is an example density of the target position. The lower panel illustrates various admissible positioning of the interceptor's reachable set $\bar{\beta}$ (i.e., the shaded areas). The $\bar{\beta}$ set is nonunique due to the unspecified control $u(\tau) \in \tau \in [t_k, t_{k+1}]$.

4. Uniqueness

The optimization (9) is in general nonconvex so that the HPI $\bar{\beta}(t_f, \hat{x}_I^\star(t_{k+1} \mid t_k))$ is nonunique. Furthermore, even when the HPI is unique, the control constraint $\hat{x}_I^\star(t_{k+1} \mid t_k)$ at its origin is in general nonunique [because the HPI is a projection of $\hat{x}_I^\star(t_{k+1} \mid t_k)$ into a lower dimensional space]. Thus, additional criteria must be imposed to select unambiguously the control constraint. In this subsection, a heuristic procedure is provided to explicitly select a unique HPI. The problem of selecting a unique control constraint from this unique HPI will then be implicitly solved in Sec. III.B.

$$U(x_I(t_{k+1} \mid t_k)) \triangleq \begin{cases} \int_{\bar{\beta}(t_f, x_I(t_{k+1}|t_k))} p(z_T \mid \mathcal{Y}^k)\, \mathrm{d}z_T, & \text{when } \bar{r}(t_k) > 0 \\ \int_{-\infty}^{\infty} \delta(z_T - z_\beta^{\max}(x_I(t_{k+1} \mid t_k))) p(z_T \mid \mathcal{Y}^k) \mathrm{d}z_T, & \text{otherwise} \end{cases} \quad (9a)$$

where

$$z_\beta^{\max}(x_I(t_{k+1} \mid t_k)) \triangleq \arg \max_{z_T \in \bar{\beta}(t_f, x_I(t_{k+1}|t_k))} p(z_T \mid \mathcal{Y}^k) \quad (9b)$$

Whenever $\bar{r}(t_k) > 0$, the $\bar{\beta}$ sets are nonempty and U is the probability that the target (at instant t_f) will remain reachable at the end of the control horizon t_{k+1}. This is illustrated in Fig. 2, where the future control strategy $u(\tau) \in [t_k, t_{k+1}]$ is yet unknown, $x_I(t_{k+1} \mid t_k)$ is one of the candidate interceptor's states, and $x_I^\star(t_{k+1} \mid t_k)$ is the one that maximizes the probability of reaching the target at t_f (despite the bounded control and the temporal evolution of the PDF). Whenever $\bar{r}(t_k) \leq 0$, the set $\bar{\beta}$ is empty, meaning that reachability of the target at t_{k+1} cannot be guaranteed (i.e., any of the modes in the current PDF can escape out of the reachable set after arrival of the future measurements). Then, U is rather selected to be the probability of interception (i.e., a second best choice because that does not account for the arrival of future measurements). This probability of interception is maximized at $z_\beta^{\max}$.

In general, an approximate calculation of the solution $\hat{x}_I^\star(t_{k+1} \mid t_k)$ to Eq. (9) can be obtained by first calculating the utility U for several admissible $\bar{\beta}$ sets and by adopting the maximizing set. The maximizing set is referred to as the highest probability interval (HPI) and its origin point is $\hat{x}_I^\star(t_{k+1} \mid t_k)$. For some functional forms of $p(z_T \mid \mathcal{Y}^k)$, the maximizing set can be calculated analytically; see Proposition IV.1 of Sec. IV for the Gaussian density case.

Let there be m HPIs and let them form the set Ω. A heuristic to select a unique HPI in Ω is proposed by adding the objective of maximizing the "robustness" of the solution with respect to the temporal evolution of the density $p(z_T \mid \mathcal{Y}^k)$. By maximized robustness, it is meant that the target could be maintained in the reachable set of the interceptor in the unforeseen event of a temporal evolution of the density larger than $\gamma(t_k)$; see Eq. (4).

The heuristic involves at most four repetitive steps. First, wherever there is an overlap in the HPIs, the set Ω is partitioned into subsets, $\Omega = \{\omega_1, \ldots, w_q\}$, $q \leq m$. This partition indicates areas of the PDF where a larger $\gamma(t_k)$ could potentially be accommodated for. Second, one of the subsets is randomly selected that avoids introducing a bias in the solution. Whenever there is only one HPI in this selected subset, uniqueness is achieved and no further steps are required. Third, the measure of the HPIs in the selected subset is reduced by a given factor ϵ, $0 < \epsilon < 1$; from Eq. (6), reducing the measure of the HPIs implies allowing for a larger uncertainty in the evolution of the PDF. Fourth, Eq. (9) is reoptimized with respect to these intervals of reduced measure. Only the HPIs of reduced measure that still maximizes Eq. (9) are preserved from one repetition to another.

This heuristic fosters a reduction in the number of HPIs, but may fail to find a unique HPI after n repetitions. Then, an arbitrary selection is made (like in a conventional MAP estimate that also suffers nonuniqueness). The latter can happen when the PDF has

multiple identically shaped peaks. The adopted procedure has similarities with that adopted in [8].

B. Calculation of the Open-Loop Control Command

The feasible control command, $u(\tau)$, $\tau \in [t_k, t_{k+1}]$, that satisfies the terminal constraint $x_I(t_{k+1}) = \hat{x}_I^\star(t_{k+1} \mid t_k)$ is in general nonunique. The control command is selected unambiguously by imposing the additional request that such control be constant (or piecewise constant) over the interval $[t_k, t_{k+1}]$. Uniqueness is then claimed *with respect to this class of constant (or piecewise-constant) controls* which achieve the steering objective. This unambiguous control is calculated by application of Theorem III.1 below. Whenever the assumptions of Theorem III.1 are satisfied everywhere in the interval $[t_k, t_{k+1}]$, the resulting control signal is constant and respects the hard constraint on the control effort. Otherwise, Theorem III.1 is applied to a sequence of subintervals in $[t_k, t_{k+1}]$ that satisfies the assumptions; the resulting control signal is piecewise constant with as many pieces as the number of subintervals.

Furthermore, application of Theorem III.1 solves implicitly the problem of selecting a unique terminal constraint $\hat{x}_I^\star(t_{k+1} \mid t_k)$ from a unique HPI $\bar{\beta}(t_f, \hat{x}_I^\star(t_{k+1} \mid t_k))$. It is achieved by guaranteeing that the state of the interceptor at the end of the receding control horizon projects onto the HPI $\bar{\beta}(t_f, \hat{x}_I^\star(t_{k+1} \mid t_k))$. This state at the end of the receding control horizon is unique by virtue of the uniqueness of the control signal delivered by the theorem.

In Theorem III.1, the following open-loop terminal cost function J^{OL} is considered:

$$J^{\mathrm{OL}}(t_k) \triangleq |\hat{z}_I^{\mathrm{HPI}}(t_k) - \bar{z}_I(t_{k+1} \mid t_k)| \tag{10a}$$

where

$$\hat{z}_I^{\mathrm{HPI}}(t_k) \triangleq D_I \Phi(t_f, t_{k+1}) \hat{x}_I^\star(t_{k+1} \mid t_k) \tag{10b}$$

$$\bar{z}_I(t_{k+1} \mid t_k) \triangleq D_I \Phi(t_f, t_{k+1}) x_I(t_{k+1} \mid t_k) \tag{10c}$$

$$= D_I \left(\Phi(t_f, t_k) x_I(t_k) + \int_{t_k}^{t_{k+1}} \Phi(t_f, \tau) B_1(\tau) u^{\mathrm{OL}}(\tau)\, \mathrm{d}\tau \right) \tag{10d}$$

In the above, $\hat{z}_I^{\mathrm{HPI}}$ and $\bar{z}_I$ are ballistic projections** (from the end of the receding control horizon) of the control constraint and of the interceptor's state, respectively. Only $\bar{z}_I$ is a function of the control signal u^{OL}. Note that $\hat{x}_I^\star(t_{k+1} \mid t_k)$ *does not have to be calculated explicitly* because the value of $\hat{z}_I^{\mathrm{HPI}}$ is

$$\hat{z}_I^{\mathrm{HPI}}(t_k) = z^{c\star}(t_k) \tag{10e}$$

where $z^{c\star}$ is the center of the HPI, $\bar{\beta}(t_f, \hat{x}_I^\star(t_{k+1} \mid t_k))$. The open-loop control signal is then calculated by application of Theorem III.1 in which $g(t_k) = \hat{z}_I^{\mathrm{HPI}}$ and $f(t_{k+1}) = D_I \Phi(t_f, t_{k+1})$.

Theorem III.1: Consider a linear system with state $x_I(\tau) \in \mathbb{R}^p$, transition matrix Φ, scalar input signal $u^{\mathrm{OL}}(\tau) \in \mathbb{R}^1$, and input matrix B_I. Consider the following control problem:

$$\inf_{u^{\mathrm{OL}} \in \mathcal{A}_u} |g(t_k) - f(t_{k+1}) x_I(t_{k+1})| \tag{11a}$$

$$\mathcal{A}_u \triangleq \{u^{\mathrm{OL}} \in \mathcal{L}^2[t_k, t_{k+1}] \mid |u^{\mathrm{OL}}(\tau)| \le u^{\max}, t \in [t_k, t_{k+1}]\} \tag{11b}$$

where only $x_I(t_{k+1})$ is a function of the control signal $u^{\mathrm{OL}}(\tau) \in [t_k, t_{k+1}]$, and the functions $f\colon \mathbb{R}^1 \to \mathbb{R}^{1\times p}$ and $g\colon \mathbb{R}^1 \to \mathbb{R}^1$ are known.

Let the function $\xi(\tau)\colon [t_k, t_{k+1}] \to \mathbb{R}^1$ be defined as

$$\xi(\tau) \triangleq f(t_{k+1}) \Phi(t_{k+1}, \tau) B_I(\tau), \qquad \tau \in [t_k, t_{k+1}] \tag{12}$$

Assume that Φ and B_I are continuous matrices of time. Assume that ξ is not identically zero and does not change sign. Then there exists an optimal control with constant value $u^{\mathrm{OL}}(\tau) = u_d^\star(t_k)$, $\tau \in [t_k, t_{k+1}]$ that solves Eq. (11) with respect to any other control in $\mathcal{A}_u$. Moreover, $u_d^\star$ is the only minimizer with a constant value and is calculated to be

$$u_d^\star(t_k) = \begin{cases} K(t_k)/\zeta(t_k), & \text{if } |K(t_k)/\zeta(t_k)| \le u^{\max}, \\ u^{\max} \mathrm{sgn}(K(t_k)/\zeta(t_k)), & \text{otherwise} \end{cases} \tag{13a}$$

where

$$K(t_k) \triangleq g(t_k) - f(t_{k+1}) \Phi(t_{k+1}, t_k) x_I(t_k) \tag{13b}$$

$$\zeta(t_k) \triangleq \int_{t_k}^{t_{k+1}} \xi(\tau)\, \mathrm{d}\tau \tag{13c}$$

Proof: Without loss of generality, suppose that $\inf_{u^{\mathrm{OL}} \in \mathcal{A}_u} |g(t_k) - f(t_{k+1}) x_I(t_{k+1})| = c$. By virtue of linearity, the relation between $x_I(t_k)$ and $x_I(t_{k+1})$ implies that

$$c = \inf_{u^{\mathrm{OL}} \in \mathcal{A}_u} |K(t_k) + \rho(u^{\mathrm{OL}})|, \qquad \rho(u) \triangleq -\int_{t_k}^{t_{k+1}} \xi(\tau) u^{\mathrm{OL}}(\tau)\, \mathrm{d}\tau \tag{14}$$

where only ρ is a function of the control signal. By virtue of the assumption that Φ and B_I are continuous, the function $\rho\colon \mathcal{A}_u \to \mathcal{R}(\rho)$ has a compact range.

Case 1. Assume that $c \neq 0$, then by virtue of compactness of ρ

$$c = \min\{|K(t_k) + \rho^{\min}|, |K(t_k) + \rho^{\max}|\} \tag{15a}$$

where

$$\rho^{\min} \triangleq \inf_{u^{\mathrm{OL}} \in \mathcal{A}_u} \rho(u^{\mathrm{OL}}) \tag{15b}$$

$$\rho^{\max} \triangleq \sup_{u^{\mathrm{OL}} \in \mathcal{A}_u} \rho(u^{\mathrm{OL}}) \tag{15c}$$

By virtue of the assumption that ξ does not change sign and is not identically zero, it follows from Eq. (14) that

$$\rho^{\min} = -u^{\max} \left| \int_{t_k}^{t_{k+1}} \xi(\tau)\, \mathrm{d}\tau \right| = -u^{\max} |\zeta(t_k)| \tag{16a}$$

$$\rho^{\max} = u^{\max} \left| \int_{t_k}^{t_{k+1}} \xi(\tau)\, \mathrm{d}\tau \right| = u^{\max} |\zeta(t_k)| \tag{16b}$$

Consequently, when $K(t_k) > 0$ and $c \neq 0$, the infimum is uniquely given by $c = |K(t_k) + \rho^{\min}|$. From Eq. (14), the unique optimal control is then

$$u^{\mathrm{OL}}(\tau) = \begin{cases} u^{\max} & \text{if } \zeta(t_k) > 0, \\ -u^{\max} & \text{if } \zeta(t_k) < 0, \end{cases} \quad \tau \in [t_k, t_{k+1}], \quad \text{if } c \neq 0, \quad K(t_k) > 0 \tag{17a}$$

When $K(t_k) < 0$ and $c \neq 0$, the infimum is uniquely given by $c = |K(t_k) + \rho^{\max}|$ and the unique optimal control is

$$u^{\mathrm{OL}}(\tau) = \begin{cases} -u^{\max} & \text{if } \zeta(t_k) > 0, \\ u^{\max} & \text{if } \zeta(t_k) < 0, \end{cases} \quad \tau \in [t_k, t_{k+1}], \quad \text{if } c \neq 0, \quad K(t_k) < 0 \tag{17b}$$

Hence, the infimum is achieved by a unique control $u^{\mathrm{OL}} \in \mathcal{A}_u$ with constant value $u_d^\star(t_k)$

$$u_d^\star(t_k) = u^{\max} \mathrm{sgn}(K(t_k)/\zeta(t_k)) \tag{18}$$

Case 2. Assume that $c = 0$. Let $\mathcal{A}_{d,u}$ be the set of control functions with constant value

**That is, projections that assume a zero control strategy $u(\tau) = 0$, $\tau \in [t_{k+1}, t_f]$.

$$\mathcal{A}_{d,u} \triangleq \{u^{\mathrm{OL}}(\tau) = u_d \mid u_d \in \mathbb{R}^1, |u_d| \leq u^{\max}, \tau \in [t_k, t_{k+1}]\} \quad (19)$$

Hence, $\mathcal{A}_{d,u} \subset \mathcal{A}_u$ and necessarily its range is $\rho(\mathcal{A}_{d,u}) \subset \rho(\mathcal{A}_u)$. By virtue of compactness, the range of $\rho(\mathcal{A}_u)$ is onto the interval $\rho(\mathcal{A}_u) = [\rho^{\min}, \rho^{\max}]$, with $\rho^{\min}$ and $\rho^{\max}$ calculated by Eq. (16). Additionally, by virtue that 1) $\rho(u_c^{\mathrm{OL}}) = u_d\zeta(t_k)$, for all $u_c^{\mathrm{OL}} \in \mathcal{A}_{u,d}$, and 2) u_d takes value in the compact set $[-u^{\max}, u^{\max}]$, the range of $\rho(\mathcal{A}_{d,u})$ is also onto the interval $\rho(\mathcal{A}_{d,u}) = [\rho^{\min}, \rho^{\max}]$. Thus, $\rho(\mathcal{A}_{d,u}) = \rho(\mathcal{A}_u)$.

By definition of the infimum, it necessarily exists a sequence of control functions $u_i^{\mathrm{OL}} \in \mathcal{A}_u$, $i = 1, \ldots$, which generates the infimum, meaning

$$\rho\left(u_i^{\mathrm{OL}}\right) \to -K(t_k), \quad \text{as } i \to \infty \quad (20)$$

Because $\rho(\mathcal{A}_u)$ and $\rho(\mathcal{A}_{d,u})$ have the same compact range, it necessarily follows that there exists a sequence $u_{c,i}^{\mathrm{OL}} \in \mathcal{A}_{d,u}$ which also generates the same infimum, meaning

$$\rho\left(u_{c,i}^{\mathrm{OL}}\right) \to -K(t_k), \quad \text{as } i \to \infty \quad (21)$$

Thus, existence of an optimal control with constant value is demonstrated.

Uniqueness of the optimal constant control is demonstrated as follows. By virtue of the assumption that ξ is not identically zero and does not change sign, there is a one-to-one relation between the domain $\mathcal{A}_{d,u}$ and the range $\rho(A_{d,u})$. That is, the function $\rho(u_{c,i}^{\mathrm{OL}})$ is uniquely inverted by

$$u_{c,i}^{\mathrm{OL}} = -\rho\left(u_{c,i}^{\mathrm{OL}}\right)/\zeta(t_k), \quad \text{for all } u_{c,i}^{\mathrm{OL}} \in \mathcal{A}_{d,u} \quad (22)$$

Then, as the domain and the range of $\rho(\mathcal{A}_{d,u})$ are compact, the function $\rho(u_{c,i}^{\mathrm{OL}})$ is homeomorphic. Thus, there is a unique optimal control with constant value, and this value is

$$u_d^\star(t_k) = K(t_k)/\zeta(t_k) \quad (23)$$

Finally, the infimum in Eq. (11) is found by first computing $K(t_k)/\zeta(t_k)$ and by determining if that satisfies the prespecified bound $u^{\max}$. If this is so, then $u_d^\star(t_k) = K(t_k)/\zeta(t_k)$ is indeed the minimizing control. Otherwise, $u_d^\star(t_k)$ in Eq. (18) is the minimizing control which, however, delivers a nonzero cost, thatis, $c \neq 0$. □

IV. Analysis

The proposition and the corollary below provide the center point $z^{c\star}$ of the optimal set maximizing Eq. (9) when the PDF is symmetric and concave (e.g., like a Gaussian density).

Proposition IV.1: Assume that the density $p(z_T \mid \mathcal{Y}^k)$ is strictly concave and symmetric around its only mode c_1. Then, the feasible HPI maximizing Eq. (9) is unique.

Moreover, the center of the HPI is $z^c(t_k) = c_1(t_k)$ whenever a $\bar{\beta}$ set with this center is feasible. Otherwise, the center of the HPI is from the $\bar{\beta}$ set whose center is the closest to c_1. The latter set is either the one containing the upper boundary of $\beta(t_f, x_I(t_k))$ (its center is z^c_{up}), or the one that contains the lower boundary of $\beta(t_f, x_I(t_k))$ (its center is z^c_{down}). Thus,

$$z^{c\star}(t_k) = \begin{cases} c_1(t_k), & \text{if feasible} \\ \arg \min\limits_{z^c \in \{z^c_{\mathrm{up}}, z^c_{\mathrm{down}}\}} |z^c(t_k) - c_1(t_k)|, & \text{otherwise} \end{cases} \quad (24)$$

Proof: Because the PDF is strictly concave and symmetric around the central point c_1, and because each $\bar{\beta}$ set is compact, it necessary follows that the optimal set $\bar{\beta}(t_f, \hat{x}_I^\star(t_{k+1} \mid t_k))$ is unique and centered on the maxima of the PDF whenever feasible. Then, $z^{c\star}(t_k) = c_1(t_k)$.

When the unconstrained maximizer is not feasible, and the constrained optimization problem is concave, it is a standard result that the feasible maximizer lies on the boundary of the feasible set. There are only two such sets because any $\bar{\beta}$ set must be nested with $\beta(t_f, x_I(t_k))$

$$\bar{\beta}(t_f, x_I(t_{k+1} \mid t_k)) \subset \beta(t_f, x_I(t_k)) \quad (25)$$

For this reason, the optimal set $\bar{\beta}(t_f, \hat{x}_I^\star(t_{k+1} \mid t_k))$ maximizing Eq. (9) has to be one of the two feasible sets containing a boundary of $\beta(t_f, x_I(t_k))$ as seen in Fig. 2. The proof that the reachable sets are nested over time is available in [7]. □

Corollary IV.2: Under the assumptions of Proposition IV.1, the center of the optimal set, $z^{c\star}$, is

$$z^{c\star} = E(p(z_T \mid \mathcal{Y}^k)) = \arg \max_{z_T} p(z_T \mid \mathcal{Y}^k) = c_1 \quad (26)$$

whenever c_1 is feasible. The first operation $E(p(z_T \mid \mathcal{Y}^k))$ delivers the MMSE estimate, and the second operation $\arg\max_{z_T} p(z_T \mid \mathcal{Y}^k)$ delivers the MAP estimate.

Proof: By virtue of the concavity and symmetric assumptions, the average and the maximum of the PDF are located at the central point c_1. □

To summarize, the control in feedback with the estimate $\hat{z}_I^{\mathrm{HPI}}$ is equivalent to controls in feedback with the MMSE and MAP estimates whenever the PDF is concave symmetric.

V. Example

The homing efficiency of the proposed predictive guidance law is studied in a specific example of a linear, constant velocity, terminal planar engagement between an interceptor and a target. For simplicity, the maneuvering dynamics of the interceptor and target are approximated by first-order transfer functions.

The target deploys decoys during the engagement. The decoys have a signature similar to that of the target, that is, the decoys appear as apparent targets to the interceptor. The interceptor is equipped with a discriminator to identify the decoys, but there is an inherent time delay for discrimination as sufficient information about the apparent targets must be gathered before discrimination. For simplicity, it is assumed that the discrimination delay δ_d is constant, meaning that the decoy $i \in S$ (launched at instant t^i_{start}) is discriminated at instant $t^i_{\mathrm{end}} = t^i_{\mathrm{start}} + \delta_d$. Results are provided for $\delta_d \in \{1.0, 3.0, 5.0\}$ s. Results are also presented in situations where the target deploys 1) a single decoy at instant t^1_{start}, and 2) a sequence of two decoys; for simplicity, it is assumed that the second decoy launches 1 s after the first decoy, that is, $t^2_{\mathrm{start}} = t^1_{\mathrm{start}} + 1$ s. For example, if $\delta_d = 3.0$ s and $t^1_{\mathrm{start}} = 5$ s, then the first decoy is deployed at $t = 5$ s, and the second decoy is deployed at $t = 6$ s. There are two decoys simultaneously present in the time interval $t \in [6, 8]$ s, and at $t = 8$ s, the first decoy is discriminated, while that happens at $t = 9$ s for the second decoy.

The adopted statistical performance criterion is the probability of a successful interception calculated through Monte Carlo simulations. An interception is deemed successful when the miss distance is within the lethal radius (LR) of the interceptor; whenever appropriate, it is assumed that $LR = 2$ m. The Monte Carlo simulation repeats the pursuit–evasion scenario 10,000 times. Each repetition has a different noise realization and a randomly selected launched time instant t^1_{start} for the first decoy.

A. Model

The geometry of the engagement is illustrated in Fig. 3. The interceptor's dynamics is linearized along the initial line of sight (at $t = 0$ s) and takes the form of Eq. (1a) with

$$A_I = \begin{bmatrix} 0 & 1 & 0 \\ 0 & 0 & 1 \\ 0 & 0 & \frac{-1}{\tau_I} \end{bmatrix}, \qquad B_I = \begin{bmatrix} 0 \\ 0 \\ \frac{1}{\tau_I} \end{bmatrix} \quad (27)$$

and where the state vector is $x_I = [\, y_I \quad \dot{y}_I \quad a_I \,]^T$. Let Φ be the state transition matrix. The set of positions reachable by the interceptor β in the interval $[t_k, t_f]$ is given by

$$\beta(t_f, x_P(t_k)) \triangleq [\beta^{\min}, \beta^{\max}] \quad (28a)$$

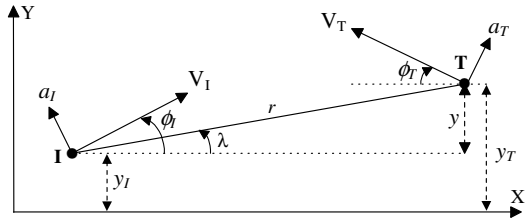

Fig. 3 Planar engagement geometry. The interceptor is denoted by "I" and the target by "T." The angles ϕ_I and ϕ_T are the respective heading angles, and λ is the line-of-sight angle. The acceleration a_I (respectively, a_T) is applied perpendicularly to the velocity vector of the interceptor V_I (respectively, to the velocity of the target V_T).

$$\beta^{\min} = D_I\left(\Phi(t_f,t_k)x_I(t_k) - u^{\max}\int_{t_k}^{t_f}\Phi(t_f,\tau)B_I\,\mathrm{d}\tau\right) \tag{28b}$$

$$\beta^{\max} = D_I\left(\Phi(t_f,t_k)x_I(t_k) + u^{\max}\int_{t_k}^{t_f}\Phi(t_f,\tau)B_I\,\mathrm{d}\tau\right) \tag{28c}$$

The relations (28b) and (28c) come from the fact that the integrand $\Phi(t_f,\tau)B_I$ does not change sign in the interval $[t_k, t_f]$ when using the matrices (27).

In the linearized model, the measurement available to the interceptor is the lateral displacement (i.e., orthogonal to the line of sight) of each apparent target $y_T(t_k)$. This measurement is taken in the inertial frame of the interceptor and is corrupted by an additive Gaussian noise of variance $Q_w(t_k) = (r(t_k)\sigma)^2$, where σ is the standard deviation of the angular noise affecting the nonlinear angular measurement on the line-of-sight angle λ.

For simplicity, the dynamics of the target is assumed to be linear with

$$A_T = \begin{bmatrix} 0 & 1 & 0 \\ 0 & 0 & 1 \\ 0 & 0 & \frac{-1}{\tau_T} \end{bmatrix}, \qquad B_T = \begin{bmatrix} 0 \\ 0 \\ \frac{1}{\tau_T} \end{bmatrix} \tag{29}$$

The evasive strategy is to employ the maximal acceleration effort, $a(\tau) = a^{\max}$, $\tau \in [0, t_f]$, and to launch decoy(s). For simplicity, the decoys have the same dynamical model as the target, but employs the reverse acceleration command. The last maximizes the separation between the target and the decoys (thus, maximizing the cost of a bad target selection by the interceptor). After deployment of a decoy, the interceptor gathers an additional measurement corresponding to the (noisy) angular position of the newly deployed decoy.

The value of the parameters are as follows: interceptor's and target's velocities $V_I = 700$ m/s and $V_T = 300$ m/s, interceptor's and target's maximum accelerations $u^{\max} = 10$ g and $a^{\max} = 3$ g, interceptor's and target's actuation time constants $\tau_I = 0.5$ s and $\tau_T = 0.5$ s, initial range $r(0) = 10,000$ m, measurement sampling time interval $\Delta = 0.1$ s, and standard deviation of the angular measurement noise $\sigma = 0.1$ mrad. The velocity vectors of the interceptor and target are initially aligned with the line of sight.

B. Calculation of the PDF

The PDF of the target state is calculated by a Kalman filter. The command of the target being unknown to the interceptor, the Kalman filter employs an augmented linear model in which the target's command is approximated by a Wiener process acceleration model (WPAM); see p. 264 in [11]. The resulting augmented linear time-invariant model is

$$\dot{x}(t) = Ax(t) + B_1u(t) + B_2w(t), \qquad w \sim \mathcal{N}(0, Q_w) \tag{30a}$$

$$y(t_k) = Hx(t_k) + v(t_k), \qquad v \sim \mathcal{N}(0, Q_v) \tag{30b}$$

with

$$A = \begin{bmatrix} 0 & 1 & 0 & 0 & 0 \\ 0 & 0 & 1 & -1 & 0 \\ 0 & 0 & \frac{-1}{\tau_T} & 0 & \frac{1}{\tau_T} \\ 0 & 0 & 0 & \frac{-1}{\tau_I} & 0 \\ 0 & 0 & 0 & 0 & 0 \end{bmatrix}, \qquad B_1 = \begin{bmatrix} 0 \\ 0 \\ 0 \\ \frac{1}{\tau_I} \\ 0 \end{bmatrix}$$

$$B_2 = \begin{bmatrix} 0 \\ 0 \\ 0 \\ 0 \\ 1 \end{bmatrix} \qquad H = [\,1 \quad 0 \quad 0 \quad 0 \quad 0\,]$$

and the state vector is $x = [\,x_1 \quad x_2 \quad x_3 \quad x_4 \quad x_5\,]^T$, where x_1 is the lateral target-interceptor displacement, x_2 is the lateral relative velocity, x_3 is the target acceleration, x_4 is the interceptor acceleration, and x_5 is the WPAM process. Following [12], the power spectral density of the WPAM process is set to $Q_w = 4(a^{\max}/t_f)^2$.

Before the deployment of any of the decoys, the PDF of the target state is Gaussian. After the deployment of the decoys, the PDF of the target position is assumed to be a summation of M equiprobable Gaussian densities. At any instant t_k, the value of M is

$$M(t_k) = 1 + N_d(t_k) \tag{31}$$

where N_d is the number of undiscriminated decoys. The data association problem (induced by measurements associated with different sources) is assumed to have been solved before the filtering. Hence, each Gaussian density is the output of a Kalman filter; the inputs of the filter are the measurements associated with the corresponding apparent target.

C. Proposed Predictive Guidance Approach

The proposed predictive guidance law, denoted $\mathrm{RG}^{\mathrm{HPI}}$, requires selecting a value for the upper bound γ, and calculating the expression for the open-loop control command.

1. *Calculation of the Bound γ*

The temporal evolution of the PDF of target positions is assumed bounded from above by γ; see Eq. (4). In [9], a heuristic to calculate the bound γ accounted for the unknown target control command. A more exhaustive heuristic bound γ is adopted here that additionally accounts for the uncertainty introduced by the covariance in the current state estimate.

Let the PDF be in the form of a Gaussian sum with M modes, and let c_i, $i \in M$ be a Gaussian mode of the PDF. Let $P^i_{k|k} \in \mathbb{R}^{5\times5}$ be the covariance matrix of the Gaussian mode c_i (this covariance matrix is calculated by the Kalman filter matched to the apparent target $i \in M$; see Sec. V.B). Let the maximum modal covariance be $P^{\max}_{k|k} = P^l_{k|k}$, $l \triangleq \arg\max_{i\in M}\|P^i_{k|k}\|$. Let the covariance of the state of an apparent target, $P^{\mathrm{AT}}_{k|k} \in \mathbb{R}^{3\times3}$, be calculated as follows:

$$P^{\mathrm{AT}}_{k|k} = I_{3\times5}P^{\max}_{k|k}I^T_{3\times5}, \qquad I_{3\times5} \triangleq [I^T_{3\times3} \mid 0_{3\times2}] \tag{32}$$

where $I_{3\times3}$ is the identity matrix. Then, γ is calculated to account for the maximum control effort and for α standard deviations of the modal state estimates as follows:

$$\gamma(t_k) = \gamma_1(t_k) + \alpha\gamma_2(t_k) \tag{33a}$$

$$\gamma_1(t_k) \triangleq a^{\max}D_T\int_{t_k}^{t_f}\Phi(t_f,\tau)B_T\,\mathrm{d}\tau = a^{\max}\left(\frac{t^2_{\mathrm{go}}}{2} - \psi_T(t_{\mathrm{go}})\right) \tag{33b}$$

$$\gamma_2(t_k) \triangleq \sqrt{P^{\mathrm{AT}}_{f|k}(1|1)} = \sqrt{D_T\Phi(t_f,t_k)P^{\mathrm{AT}}_{k|k}\Phi^T(t_f,t_k)D^T_T} \tag{33c}$$

$$= \sqrt{\begin{aligned} &P^{\mathrm{AT}}_{f|k}(1,1) + t_{\mathrm{go}}P^{\mathrm{AT}}_{f|k}(1,2) + \psi_T(t_{\mathrm{go}})P^{\mathrm{AT}}_{f|k}(1,3) \\ &+ t_{\mathrm{go}}\Big(P^{\mathrm{AT}}_{f|k}(1,2) + t_{\mathrm{go}}P^{\mathrm{AT}}_{f|k}(2,2) + \psi_T(t_{\mathrm{go}})P^{\mathrm{AT}}_{f|k}(2,3)\Big) \\ &+ \psi_T(t_{\mathrm{go}})\Big(P^{\mathrm{AT}}_{f|k}(1,3) + t_{\mathrm{go}}P^{\mathrm{AT}}_{f|k}(2,3) + \psi_T(t_{\mathrm{go}})P^{\mathrm{AT}}_{f|k}(3,3)\Big) \end{aligned}} \tag{33d}$$

where γ_1 is the maximum control effort of an apparent target, γ_2 is 1 standard deviation in the estimated position of an apparent target, α is the number of standard deviations accounted for (from trials and errors, $\alpha = 2$), Φ is the transition matrix from dynamics (26), $P^{\mathrm{AT}}_{f|k}$ is the covariance matrix at the instant t_f conditioned on the $\mathcal{Y}^k$, the time to go is $t_{\mathrm{go}} \triangleq t_f - t$, the projector D_T is given in Eq. (3b), and $\psi_T(t_{\mathrm{go}}) \triangleq \tau_T t_{\mathrm{go}} - \tau_T^2(1 - e^{-t_{\mathrm{go}}/\tau_T})$.

2. *Open-Loop Control Command*

The interceptor with dynamics (27) satisfies the assumptions of Theorem III.1 and the open-loop control command has a constant value in any receding interval, $u^{\mathrm{OL}}(\tau) = u_d^\star(t_k)$, $\tau \in [t_k, t_{k+1}]$. This constant value $u_d^\star$ is given by Eq. (13a) in which

$$K(t_k) = \hat{z}_I^{\mathrm{HPI}}(t_k) - \Big(y_I(t_k) + \dot{y}_I(t_k)t_{\mathrm{go}} + a_I(t_k)\Big[\tau_I t_{\mathrm{go}} + \tau_I^2(e^{-t_{\mathrm{go}}/\tau_I} - 1)\Big]\Big) \tag{34a}$$

$$\zeta(t_k) = \Delta(t_{\mathrm{go}} - \tau_I) + \tau_I^2 e^{-t_{\mathrm{go}}/\tau_I}(e^{\Delta/\tau_I} - 1) - \frac{\Delta^2}{2} \tag{34b}$$

D. Guidance Laws Employed for Comparison

Two classes of guidance laws are used for comparison. The first class employs the controller proposed in Sec. III.B but with a conventional feedback signal, instead of the receding HPI control constraint. The conventional feedback signals considered are the MMSE and the MAP estimates. The resulting laws are denoted $\mathrm{PG}^{\mathrm{MMSE}}$ and $\mathrm{PG}^{\mathrm{MAP}}$, respectively. The adequacy of the HPI estimate [that maximizes Eq. (9)] can be evaluated by comparing these latter two laws with the proposed predictive guidance law.

The second class of guidance laws is represented by the proportional navigation (PN) law (a law with fixed cost and control horizons) in feedback with the MMSE and MAP estimates. The resulting laws are denoted $\mathrm{PN}^{\mathrm{MMSE}}$ and $\mathrm{PN}^{\mathrm{MAP}}$, respectively. The navigation constant of the PN law is selected to have value $N' = 3$; see Chapter 2 in [2].

E. Numerical Results

1. *Example Trajectories*

In Fig. 4, the interceptor and target trajectories are illustrated in two example engagements. In both cases, a single decoy is deployed by the target and the discrimination delay is $\delta_d = 3.0$ s. In the first example (upper panel), the decoy is deployed at $t^1_{\mathrm{start}} = 2$ s, while the decoy is deployed at $t^1_{\mathrm{start}} = 4$ s in the second example (lower panel). Before the launch of the decoy, that is, at $t \in [0, t^1_{\mathrm{start}}]$, the PDF is Gaussian and the laws $\mathrm{RG}^{\mathrm{HPI}}$, $\mathrm{RG}^{\mathrm{MMSE}}$, and $\mathrm{RG}^{\mathrm{MAP}}$ steer the interceptor along the same trajectory, in accordance with Corollary IV.2. In the interval $t \in [t^1_{\mathrm{start}}, t^1_{\mathrm{end}}]$, there are two apparent targets (equally probable) from the point of the view of the interceptor. Then, the $\mathrm{RG}^{\mathrm{MMSE}}$ law (dashed line) steers the interceptor toward the centroid location; the $\mathrm{RG}^{\mathrm{MAP}}$ law (dotted line) randomly picks one of the apparent targets and steers the interceptor toward it; and the $\mathrm{RG}^{\mathrm{HPI}}$ law steers the interceptor on a trajectory that keeps both apparent targets reachable. After discrimination, at $t \in [t^1_{\mathrm{end}}, t_f]$, the three laws steer the interceptor toward the target.

In Fig. 4a, the interceptor with the $\mathrm{RG}^{\mathrm{MAP}}$ law misses the target because the wrong apparent target was picked (a 50% probability event) and there is not sufficient time left to recover after discrimination. The interceptor using the $\mathrm{RG}^{\mathrm{MMSE}}$ law succeeds, because it has sufficient time left after discrimination to steer the interceptor on an interception trajectory. The interceptor with the $\mathrm{RG}^{\mathrm{HPI}}$ law also succeeds because both the target and the decoy are still in the reachable set of the interceptor at the discrimination time.

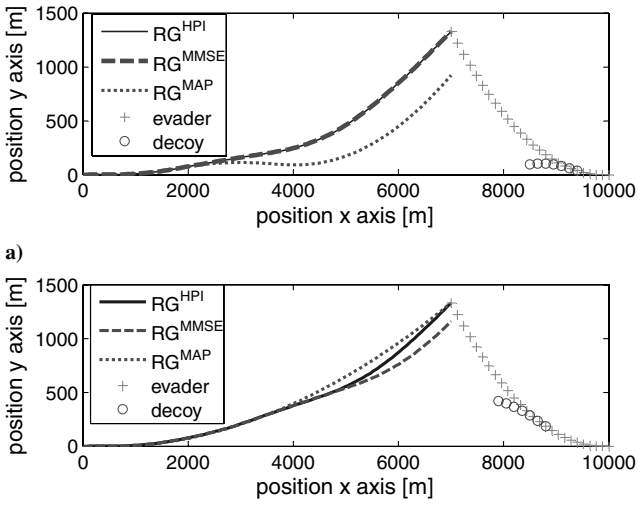

a)

b)

Fig. 4 Trajectories in an example engagement with a single decoy and a discrimination delay $\delta_d = 3.0$ s. The deployment and discrimination time of the decoy are a) upper panel: $t^1_{\mathrm{start}} = 2$ s and $t^1_{\mathrm{end}} = 5$ s, and b) lower panel: $t^1_{\mathrm{start}} = 4$ s and $t^1_{\mathrm{end}} = 7$ s. The interceptor is initially at the bottom left corner and the target is initially at the bottom right corner.

In Fig. 4b, the interceptor with the $\mathrm{RG}^{\mathrm{MAP}}$ law (dotted line) intercepts the target because the right apparent target was fortuitously chosen in the interval $t \in [t^1_{\mathrm{start}}, t^1_{\mathrm{end}}]$ (a 50% probability event). The interceptor with the $\mathrm{RG}^{\mathrm{MMSE}}$ law (dashed line) misses because there is not sufficient time left in the interval $t \in [t^1_{\mathrm{end}}, t_f]$ to steer the interceptor on the new interception trajectory. The interceptor employing the $\mathrm{RG}^{\mathrm{HPI}}$ law first employs a cautious trajectory that keeps both apparent targets reachable. However, this cautious trajectory is abandoned *before* discrimination when one of the two apparent targets threaten to become unreachable. One of the apparent targets is then randomly selected. In the example, the right apparent target is selected (a 50% probability event) and the interception is successful.

2. *Probability of Interception: One Decoy*

The probability of interception (PI) is shown in Fig. 5 for three discrimination delays, and for the laws $\mathrm{RG}^{\mathrm{HPI}}$, $\mathrm{RG}^{\mathrm{MMSE}}$, and $\mathrm{RG}^{\mathrm{MAP}}$. In the left panels, a LR = 2 m is assumed, and the PI versus the deployment instant of the decoy, t^1_{start}, is illustrated. In the right panels, t^1_{start} is assumed uniformly distributed, and the PI versus LR is displayed.

In the left panels, for $t^1_{\mathrm{start}} \approx [9.2, 10]$, PI = 1.0 in all cases because there is not sufficient time left in the engagement for the decoy to affect the outcome. The details of the curves with $\delta_d = 3.0$ s in Fig. 5c are explained as follows. The interceptor employing $\mathrm{RG}^{\mathrm{MMSE}}$ when $t_{\mathrm{start}} \approx [0.0, 2.5]$ s has PI = 1.0 because there is sufficient time left after discrimination to steer the interceptor's trajectory on an interception course. Conversely, when $t_{\mathrm{start}} \approx [2.5, 9.2]$ s, the interceptor with $\mathrm{RG}^{\mathrm{MMSE}}$ has PI = 0.0 because there is not sufficient time left for a trajectory correction after discrimination. The interceptor employing $\mathrm{RG}^{\mathrm{MAP}}$ when $t_{\mathrm{start}} \approx [0.0, 9.2]$ s has PI = 0.5 because there is not sufficient time left in the engagement to recover from a wrongly chosen apparent target. The interceptor employing $\mathrm{RG}^{\mathrm{HPI}}$ exhibits PI = 1.0 for $t_{\mathrm{start}} \approx [0.0, 2.5]$ s because it employs a cautious trajectory, while it exhibits PI = 0.5 for $t_{\mathrm{start}} \approx [2.5, 9.2]$ s because one of the two apparent targets must then be selected randomly. The curves with $\delta_d = 5.0$ s and $\delta_d = 1.0$ are similarly explained.

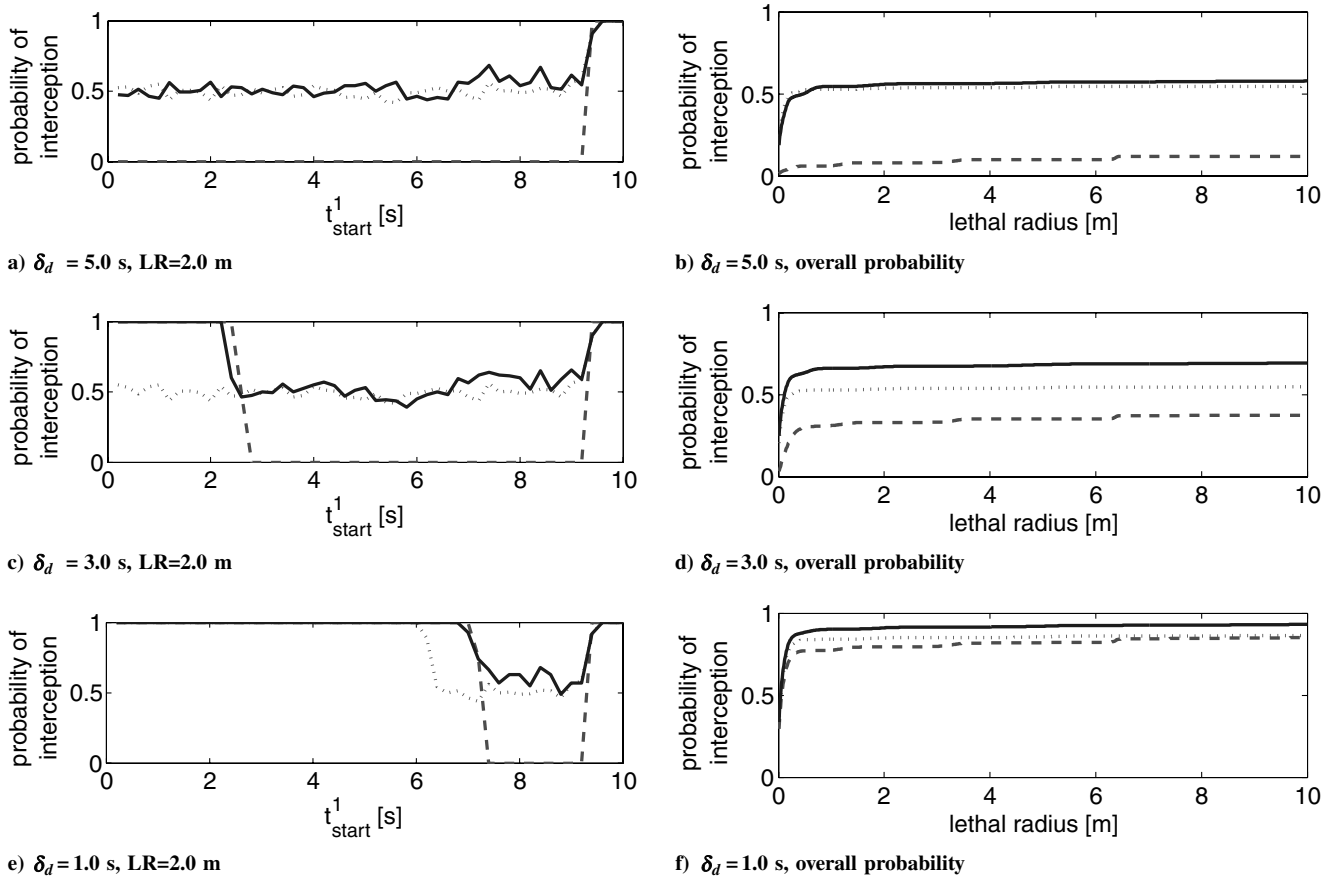

a) δ_d = 5.0 s, LR=2.0 m

b) δ_d = 5.0 s, overall probability

c) δ_d = 3.0 s, LR=2.0 m

d) δ_d = 3.0 s, overall probability

e) δ_d = 1.0 s, LR=2.0 m

f) δ_d = 1.0 s, overall probability

Fig. 5 Interception probability with a single decoy. Left panels: interception probability vs the deployment instant of the decoy (it is assumed that LR = 2 m). Right panels: interception probability vs the lethal radius (assuming that t^1_{start} is uniformly distributed). The delay for discrimination is $\delta_d = 1.0$ s (lower panels), $\delta_d = 3$ s (middle panels), and $\delta_d = 5.0$ s (upper panels). The curves are RG^{HPI} (solid lines), RG^{MMSE} (dashed lines), and RG^{MAP} (dotted lines).

In the right panels, the overall probability of interception is interpreted as follows. Consider Fig. 5d, the overall probability of interception for LR = 2 m is 67% using RG^{HPI}, 54% using RG^{MAP}, and 33% using RG^{MMSE}. Moreover, this probability is approximately constant for any LR $\in$ [0.5, 10] m. In t Figs. 5d and 5f, the RG^{HPI} law delivers the higher overall probability of interception. In the case of Fig. 5b, the RG^{HPI} and RG^{MAP} have a similar probability of interception because the discrimination delay is too long, that is, the RG^{HPI} cannot maintain both the target and the decoy in the reachable set until discrimination (one of the two apparent targets has to be randomly chosen).

3. *Probability of Interception: Two Decoys*

The PI in scenarios with two decoys is given in Fig. 6 for the cases with $\delta_d = 1$ s and $\delta_d = 3$ s. The two decoys are launched in sequence: the first decoy is launched at instant t^1_{start} and the other is launched 1 s later, at $t^2_{start} = t^1_{start} + 1$ s. In the case of the discrimination delay $\delta_d = 1$ s, the second decoy appears after the discrimination of the first one. The behavior of the laws in Figs. 6c and 6d is then similar to the case with one decoy and the RG^{HPI} delivers the highest PI. In the case of the discrimination delay $\delta_d = 3$ s, the two decoys can exist simultaneously. The RG^{MAP} law has then a 33% PI (as expected) while it is 24% with the RG^{MMSE} law. However, the behavior of the RG^{HPI} law is more complex and it is not better or similar to that of the RG^{MAP} law when the first decoy is launched in the interval $t^1_{start} \in [2.3, 4]$ s. That happens for two reasons: 1) the estimator falsely assigns an equal probability to the modes when there are three simultaneous apparent targets, this despite the fact that the launch of the second decoy by the target should provide sufficient information to discriminate between the first decoy and the target, and 2) in the Monte Carlo simulation, the target is always the leftmost mode, which does not emulate a situation in which the three apparent targets are equiprobable. Nonetheless, the overall PI of the RG^{HPI} law remains the highest at 49%. Moreover, the expected behavior of the RG^{HPI} can be recovered by either 1) improving the estimator to handle apparent targets with unequal probabilities, or 2) matching the Monte Carlo simulation with the assumption of the current estimator by making the apparent targets truly equiprobable.

4. *Probability of Interception:* RG^{HPI} *Versus* PN

The PI of the RG^{HPI} and PN laws for $\delta_d = 3.0$ s and a single decoy is depicted in Fig. 7. The probability of interception of the RG^{HPI} law is the highest with an overall PI of 67% when LR = 2.0 m. By comparison, the overall PI is 28 and 60% with the PN^{MMSE} and PN^{MAP} laws, respectively. When LR is small, the RG^{HPI} law is even more advantageous.

5. *Summary of the Results and Remarks*

The overall PI versus the discrimination delay for LR = 2.0 m is summarized in Table 1. The overall PI of RG^{HPI} law is significantly higher than that of RG^{MMSE} and RG^{MAP} when the discrimination delay is sufficiently small, that is, for $\delta = 1.0$ s and $\delta = 3.0$ s. When the discrimination delay is larger, that is, $\delta = 5.0$ s, the RG^{HPI} law cannot maintain the target and the decoy in the reachable set of the interceptor. One of the two apparent targets is then randomly selected before discrimination and performances are similar to that of RG^{MAP}.

Notice that increasing the LR is not sufficient to increase the PI in the presence of decoys, because the overall PI in Table 1 is stable in a broad range of LR, that is, LR $\in$ [0.5, 10] m.

Finally, the results of the RG^{HPI} law were obtained with the upper bound γ selected in Eq. (33). If the value of γ would have been selected much larger, for example, $\gamma(t_k) \to \infty$, the homing

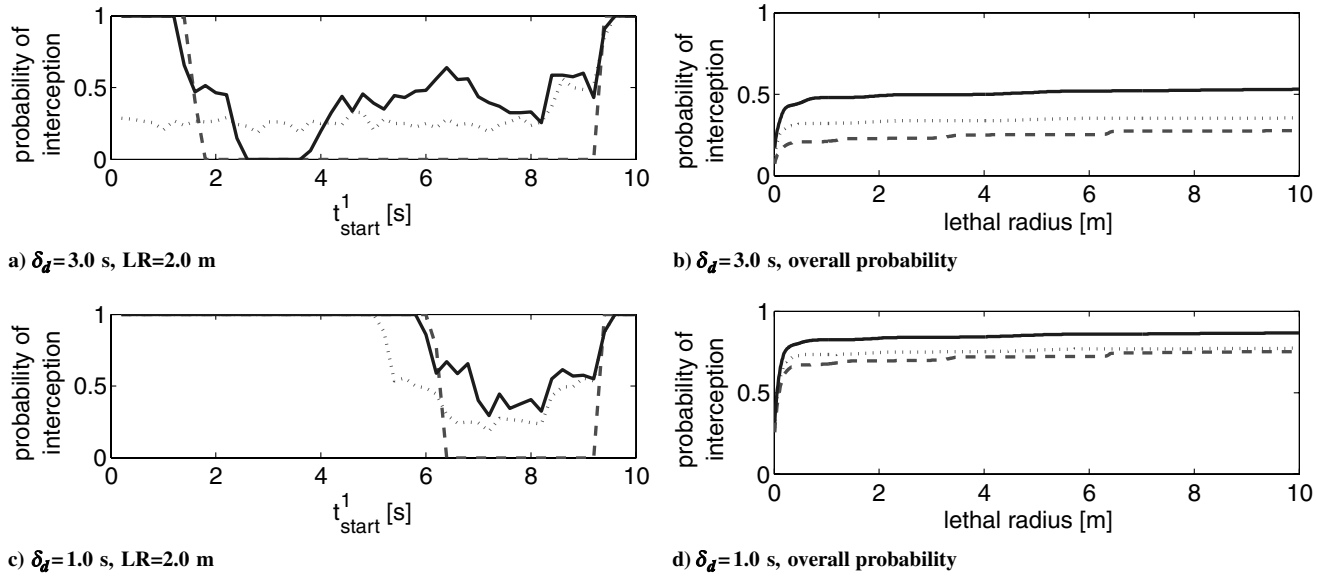

a) δ_d=3.0 s, LR=2.0 m

b) δ_d=3.0 s, overall probability

c) δ_d=1.0 s, LR=2.0 m

d) δ_d=1.0 s, overall probability

Fig. 6 Interception probability with two decoys. Left panels: interception probability vs the deployment instant of the decoy (it is assumed that LR = 2 m). Right panels: interception probability vs the lethal radius (assuming that t^1_{start} is uniformly distributed). The delay for discrimination is $\delta_d = 1.0$ s (lower panels), $\delta_d = 3$ s (middle panels), and $\delta_d = 5.0$ s (upper panels). The curves are RG^{HPI} (solid lines), RG^{MMSE} (dashed lines), and RG^{MAP} (dotted lines).

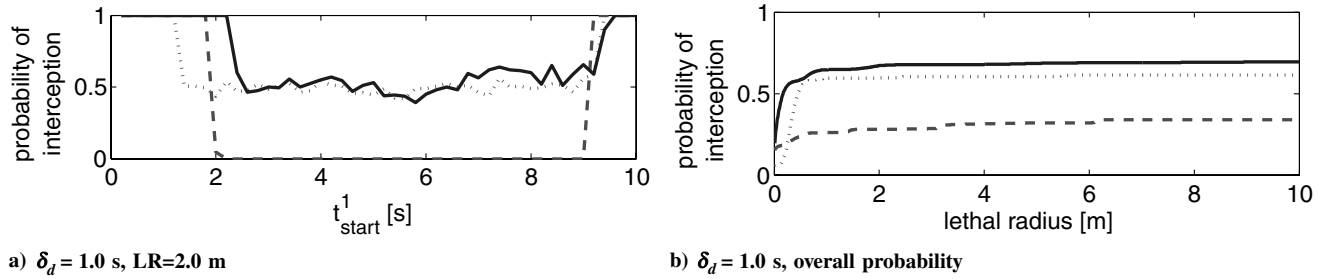

a) δ_d = 1.0 s, LR=2.0 m

b) δ_d = 1.0 s, overall probability

Fig. 7 Interception probability of the RG^{HPI} and PN laws. A single decoy is launched and $\delta_d = 3$ s. Left panels: interception probability vs the deployment instant of the decoy (the lethal radius is assumed to be LR = 2 m). Right panels: interception probability vs the lethal radius (the overall probability is shown assuming that the instant t^1_{start} is uniformly distributed). The curves are RG^{HPI} (solid lines), PN^{MMSE} (dashed lines), and PN^{MAP} (dotted lines).

performance of the RG^{HPI} law would have been similar to that of the RG^{MAP} law because it would imply that $\bar{r}(t_k) < 0$ in Eq. (9). If the value of γ would have been selected much smaller, for example, $\gamma(t_k) = 0$, the homing performance of the RG^{HPI} law degrades. The degradation happens when the temporal evolution of the PDF involves 1) an apparent target that is reachable when the density is conditioned on the σ-algebra $\mathcal{Y}^k$, and 2) this apparent target is unreachable when conditioned on $\mathcal{Y}^f$. Nonetheless, results with $\gamma(t_k) = 0$ were presented in [6] showing that the overall PI was still the highest using the RG^{HPI} law.

VI. Conclusions

A predictive guidance law that maximizes the probability of the target being present in the reachable set of the pursuer was presented. Situations where the PDF of the target position is multimodal, as encountered in the presence of decoys or when applying multiple model estimators, were of particular interest. The proposed receding horizon law was demonstrated to result into a higher interception probability than comparable laws in feedback with conventional state estimates and/or employing a fixed control horizon. The benefits of the proposed law are attributed to its ability to account for the probability density of the system's state, the unknown future measurements that will modify this probability density, and the bounded control of the interceptor.

Future topics for research in this direction could be the application of a similar law when the reachable set of the pursuer is nonlinear and suffers uncertainties, as well as studying the possibility of employing a receding cost horizon.

Table 1 Overall probability of interception vs the discrimination delay

	One decoy			Two decoys		
	RG^{HPI}	RG^{MMSE}	RG^{MAP}	RG^{HPI}	RG^{MMSE}	RG^{MAP}
$\delta = 1.0$ s	0.91	0.80	0.85	0.83	0.69	0.75
$\delta = 3.0$ s	0.67	0.33	0.54	0.49	0.23	0.33
$\delta = 5.0$ s	0.55	0.08	0.54	0.33	0.08	0.33

References

[1] Cloutier, J. R., Evers, J. H., and Feeley, J. J., "An Assessment of Air-to-Air Missile Guidance and Control Technology," *IEEE Control Systems Magazine*, Vol. 9, No. 6, Oct. 1989, pp. 27–34.

[2] Zarchan, P., *Tactical and Strategic Missile Guidance*, 4th ed., Progress in Astronautics and Aeronautics, Vol. 199, AIAA, Reston, VA, 2004.

[3] Bell, W. A., and Pringle, L. N., "The Impact of Seeker Angular Resolution on the Miss Distance of Tactical Missiles," AIAA Paper 2000-770, Jan. 2000.

[4] U.S. Department of Defense, U.S. Navy, Naval Academy, Weapons and System Engineering Department (WSED), Fundamentals of Naval Weapons Systems, Annapolis, MD, 1984, http://fas.org/man/dod-101/navy/docs/fun/index.html.

[5] Best, R. A., and Norton, J. P., "Predictive Missile Guidance," *Journal of Guidance, Control, and Dynamics*, Vol. 23, No. 3, 2000, pp. 539–546.

[6] Dionne, D., Michalska, H., and Rabbath, C. A., "A Predictive Guidance Law with Uncertain Information About the Target State," *Proceedings of the American Control Conference*, IEEE, Piscataway, NJ, June 2006, INSPEC Accession No. 9046990.

[7] Shaviv, I. G., and Oshman, Y., "Fusion of Estimation and Guidance Using Sequential Monte Carlo Methods," *Proceedings of the IEEE Conference on Control Applications*, IEEE, Piscataway, NJ, Aug. 2005, pp. 1361–1366.

[8] Shaviv, I. G., and Oshman, Y., "Guidance Without Assuming Separation," AIAA Paper 2005-6154, Aug. 2005.

[9] Dionne, D., and Rabbath, C. A., "Predictive Guidance for Pursuit-Evasion Engagements Involving Decoys," AIAA Paper 2006-6214, Aug. 2006.

[10] Striebel, C., "Sufficient Statistics in the Optimum Control of Stochastic Systems," *Journal of Mathematical Analysis and Applications*, Vol. 12, No. 3, 1965, pp. 576–592.

[11] Bar-Shalom, Y., and Li, X. R., *Estimation and Tracking: Principles, Techniques and Software*, Artech House, Inc., Boston, MA, 1993.

[12] Zarchan, P., "Representation of Realistic Evasive Maneuvers by the Use of Shaping Filters," *Journal of Guidance, Control, and Dynamics*, Vol. 2, No. 4, 1979, pp. 290–295.